Comunicações Geológicas

Versão online: https://www.lneg.pt/wp-content/uploads/2020/07/Volume_107_III.pdf

Comunicações Geológicas (2020) 107, Especial III, 21-39
ISSN: 0873-948X; **e-ISSN:** 1647-581X

Multispectral and hyperspectral remote sensing as a source of knowledge in the Portuguese sector of the Iberian Pyrite Belt

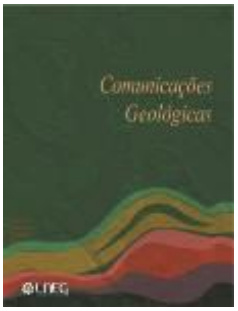

Deteção remota multiespectral e hiperespetral como fonte de conhecimento no sector português da Faixa Piritosa Ibérica

L. Quental[1*], P. Gonçalves[1], D. de Oliveira[1], M. J. Batista[1], J. X. Matos[1], A. J. Sousa[2], S. Marsh[3], J. Carreiras[4], R. Dias[1]

Artigo original
Original article

Abstract: Remote sensing is an invaluable tool to increase geological and mining knowledge, due to its screening view and variable discrimination and identification capabilities of the target materials. In this study an overview of remote sensing research developed and ongoing within the Portuguese sector of the Iberian Pyrite Belt (PSIPB) since 2000 is given. Multispectral and hyperspectral datasets were processed using hybrid methods, related both to general and detailed characterization, to: 1) support geological, mineral and hydrothermal mapping, 2) generate products derived from multivariate analysis and band ratios, 3) enhance correlation with radiometric data, 4) provide elements for environmental assessment concerning mining activity, 5) map Acid Mine Drainage (AMD) based on spectral field signatures, 6) quantify AMD based on high correlation mineralogical mapping, and 7) monitor AMD. The results highlight the importance of the quantitative digital support given by remote sensing tools within the Portuguese Sector of the Iberian Pyrite Belt (PSIPB), ruled by georesource exploitation in different stages of the Mine Lyfe Cycle.

Keywords: Multispectral, hyperspectral, Portuguese sector of the Iberian Pyrite Belt (PSIPB), multi-source data, spectral information.

Resumo: A deteção remota é uma ferramenta valiosa para aumentar o conhecimento geológico e mineiro, devido à visão sinótica e à capacidade variável de discriminação e identificação dos materiais-alvo. Neste trabalho dá-se uma visão geral da investigação através dos trabalhos de deteção remota desenvolvidos e em curso no Setor Português da Faixa Piritosa Ibérica (SPFPI) desde 2000. Os dados multiespectrais e hiperespectrais foram processados usando métodos híbridos quer para a sua caracterização geral quer detalhada para: 1) apoiar a cartografia geológica, de mineralizações e sistemas hidrotermais, 2) gerar produtos de análise multivariada e rácios de bandas, 3) melhorar a correlação com dados radiométricos 4) fornecer elementos para avaliação ambiental em áreas mineiras, 5) cartografar a drenagem ácida de mina (DAM) com assinaturas espectrais de campo, 6) quantificar a DAM através de cartografia mineralógica de alta correlação, e 7) monitorizar a DAM. Destaca-se a importância do suporte digital quantitativo dado por ferramentas de deteção remota no SPFPI, regido pela exploração de georrecursos em diferentes fases do Ciclo de Vida das Minas.

Palavras-chave: Multiespectral, hiperespetral, sector Português da Faixa Piritosa Ibérica (SPFPI), dados multi-fonte, informação espetral.

[1] Laboratório Nacional de Energia e Geologia, Apartado 7586 / 2610-999 Amadora, Portugal.
[2] CERENA, Instituto Superior Técnico, Universidade Técnica de Lisboa (TULisbon), Avenida Rovisco Pais, 1, 1049-001 Lisboa, Portugal.
[3] Faculty of Engineering. University of Nottingham. Nottingham Geospatial Building, United Kingdom.
[4] Centro de Estudos Florestais, Instituto Superior de Agronomia, Tapada da Ajuda, 1349-017 Lisboa, PORTUGAL. National Centre for Earth Observation, University of Sheffield, Western Bank, Sheffield, S10 2TN, United Kingdom.

*Corresponding author/Autor correspondente: lidia.quental@lneg.pt

1. Introduction

With screening capabilities, remote sensing adds an invaluable contribution for characterizing and monitoring various themes, including geology and geo-resources. The characterization relies on deepening the knowledge of the target area by providing quantitative information of the material´s response across the electromagnetic spectrum. The monitoring is based on repeated data acquisition for detection of a variation of parameters of interest, ranging through decades to the minimum limit of the revisit time of the satellite.

The level of extraction of information from the images is dependent upon the characteristics of the imaging sensors, particularly concerning spectral and spatial resolution, signal to noise ratio, wavelength range, and afterwards of the algorithms used in processing (Quental *et al.*, 2012).

The imaging sensors acquire information by measuring energy across the electromagnetic spectrum and convey it in an image with spectral bands. In multispectral images the number of bands varies from 3 to less than ≈ 20 discontinuous broad bands in a wide spectral range. In hyperspectral or imaging spectroscopy (IS), tens or hundreds of contiguous spectral bands collect the spectra of energy received at the sensor for each spatial unit (pixel) with high signal to noise ratio. The spectra are used to extract information based on the signature of the interaction of matter and energy. In other words, the IS data expands the point concept of spectroscopy, by gathering spatial data over large areas with high spectral resolution relying on the spectroscopy principles established in the XIXth century (Schaepman *et al.*, 2006, 2009, in Quental *et al.*, 2011).

The distinct characteristics of the sensors implies a variable level of information extracted on the targeted materials, i.e. discrimination of groups of minerals in multispectral, and mineralogical or chemical identification with hyperspectral or IS.

With the estimated extraction of several million tons of raw materials since pre-roman times, the Portuguese sector of the Iberian Pyrite Belt (PSIPB) shows distinct phases if addressed

under the point of view of Mine Life Cycle (Matos and Martins, 2006; Tornos, 2006; Matos *et al.*, 2008; Locutura, 2011). While some brownfield areas are under detailed exploration using more sophisticated tools, *e.g*. Neves-Corvo mining region EXPLORA (Matos *et al.*, 2019, 2020) and SmartExploration (Carvalho *et al.*, 2019) projects, increasing the probability of refining additional near-mine targets, others remain with a significant environmental footprint that can be addressed and researched using remote sensing tools. The possibility to get at each data capture, by airborne or spaceborne sensors, the status of a site is a key feature for mine remediation, comprehension of the pathways of the contaminants, and monitoring parameters such as Acid Mine Drainage (AMD).

The aim of this study is to provide an overview of some of the research undertaken since 2000 within the PSIPB using optical remote sensing methods, ranging from multispectral to hyperspectral (IS) datasets. The focus is on geological and mining characterization using ancillary data, as well as environmental assessment and monitoring particularly at the late stages of the Mine Life Cycle.

Through this period a paradigm shift occurred in remote sensing, with the U.S. Geological Survey making freely available all the images from the Landsat program in 2008 and the launch of Sentinel sensors of the Copernicus European Space Program in 2014 (Szantoi and Strobl, 2019). This was accompanied by successive improvements in datasets delivery and in the development of open source software.

2. Framework

2.1. Portuguese Sector of the Iberian Pyrite Belt (PSIPB)

Stratigraphically, the Iberian Pyrite Belt-IPB (Fig.1) is made up of the basal Phyllite-Quartzite Group (PQG), the Volcano-Sedimentary Complex (VSC) and capped by the Flysch Group (FG) (Fig. 1). The occurrence of dozens of massive sulphides and stockwork mineralizations in the VSC and PQG justify the classification of the IPB as a major metallogenetic province in Europe (Barriga *et al*., 1997; Tornos, 2006; Locutura, 2011).

The existing potential of the Belt in terms of mineral exploration and the continued recent discovery of new economic deposits [*e.g.* Semblana (2010) and Monte Branco (2012), La Magdalena (2013), Sesmarias (2014), Lagoa Salgada Central (2017) and Elvira (2018) (de Oliveira *et al*., this volume)], relies on certain criteria (Matos and Filipe, 2013) such as outcrop structures of the VSC and PQG and areas where these formations are hidden under later geological formations. To better define this region and augment its mineralogical potential, borehole data and also indirect methods, such as geophysical surveys, were studied, in order to identify the potential extension of the IPB basement beneath the Baixo Tejo/Alvalade and Guadalquivir cenozoic basins and also the Mértola and Mira Formations (Flysch Group, Carboniferous) (Matos *et al.*, 2020). Following these criteria, the PSIPB covers an area of 10 583 km^2 (Fig. 1).

Global studies described cover the PSIPB, whilst local detailed studies report to the Aljustrel and S. Domingos mining areas (Fig. 2).

2.2. Mining history

During Roman times, active mining operations have been reported in Rio Tinto, Tharsis, Sotiel, Aljustrel and many other localities (Pinedo-Vara, 1963). Archaeological findings such as two metal tablets discovered at Aljustrel (Portugal), recorded the Roman mining law for the province. The period of greatest mining development coincides with the Industrial Revolution during the 19th and early 20th centuries during which, more than sixty mines were extracting copper, sulphur, gold and silver, therefore, generating significant volumes of mining wastes deposited in dumps and tailings. Examples of the waste volumes are about 1,700.000 m^3 of S. Domingos and about 4,100.000 m^3 of Aljustrel, the later already in confinement in remediated areas. Several other mines in IPB were already remediated, such as Lousal where the project included a Science Interpretation Centre (Centro Ciência Viva do Lousal), generating outside interest, and mostly importantly, employment opportunities in the town (Relvas *et al.*, 2012). Presently the waste dumps may have a renewed interest as a potential source of critical raw materials for Europe (COM (2017) 490 final). Vieira *et al.* (2016, 2020) referred resources of 4.0 Mt @ 0.64 g/t Au and 7.30 g/t Ag in the São Domingos mine northern area, corresponding to a metal content of 82,878 oz t Au and 955,753 oz t Ag.

3. Datasets and objetives

3.1. Multispectral

Multispectral data analysed encompasses Landsat ETM+ (NASA, 2016), QuickBird (Digital Globe, 2019) and Sentinel 2 (ESA, 2015) of the Copernicus program. The characteristics of these images related to number of bands, wavelength centre, bandwidth and spatial resolution are depicted in table I.

Landsat ETM+ image was acquired on 4th August 2000 over south Portugal and Spain and commercially orthorectified. The main aim was to check the capabilities to assess environmental impact of the mining activities when compared with other methodologies using a contemporary sensor, 17 days apart and with similar atmospheric conditions, over the S. Domingos mining area (Quental *et al*., 2002, Quental, 2011) (Figs. 2 and 3, Tab. 2 2). Other important studies, developed afterwards, focused on the integration of geochemical data with spectral data in a regional approach considering the target areas of S. Domingos and Aljustrel (Vairinho *et al*., 2004). This image was also used to characterise the chief environmental and societal elements under threat from a spill in the Aljustrel mining area and the environmental factors controlling its dispersion (Quental 2006).

QuickBird very-high spatial resolution images, suitable to enhance image interpretability when compared with others, (Tab. 1), was acquired over the Aljustrel mining area (Fig. 2) with the purpose of environment characterization by generating a land cover focused on the prevention of dam failure of mining works (Quental, 2006). A detailed geological and mining mapping (Matos, 2006; Matos *et al.*, 2010) was another characterization undertaken.

Sentinel-2 mission is composed by a constellation of two polar-orbiting satellites placed in the same sun-synchronous orbit, acquiring information on different wavelengths and spatial resolution using a swath of 290 km and a revisit time of 5 days (constellation) and 10 days (individual satellite) (ESA, 2015; Szantoi and Strobl, 2019). The purpose of the Sentinel-2 mission is to provide continuous imaging of Earth, providing data to Copernicus Services, which include: Land cover/Land-Use changes, vegetation, soil and water monitoring and continuous observation of waterways and coastal areas.

Sentinel 2 has been used to improve the geological and mining knowledge, by generating valued added products such as geologic indices (Said *et al.*, 2019), land cover classification based on spectral information, mineral abundance mapping (Van Der Meer *et al.*, 2014) based on endmembers extraction (Mylon

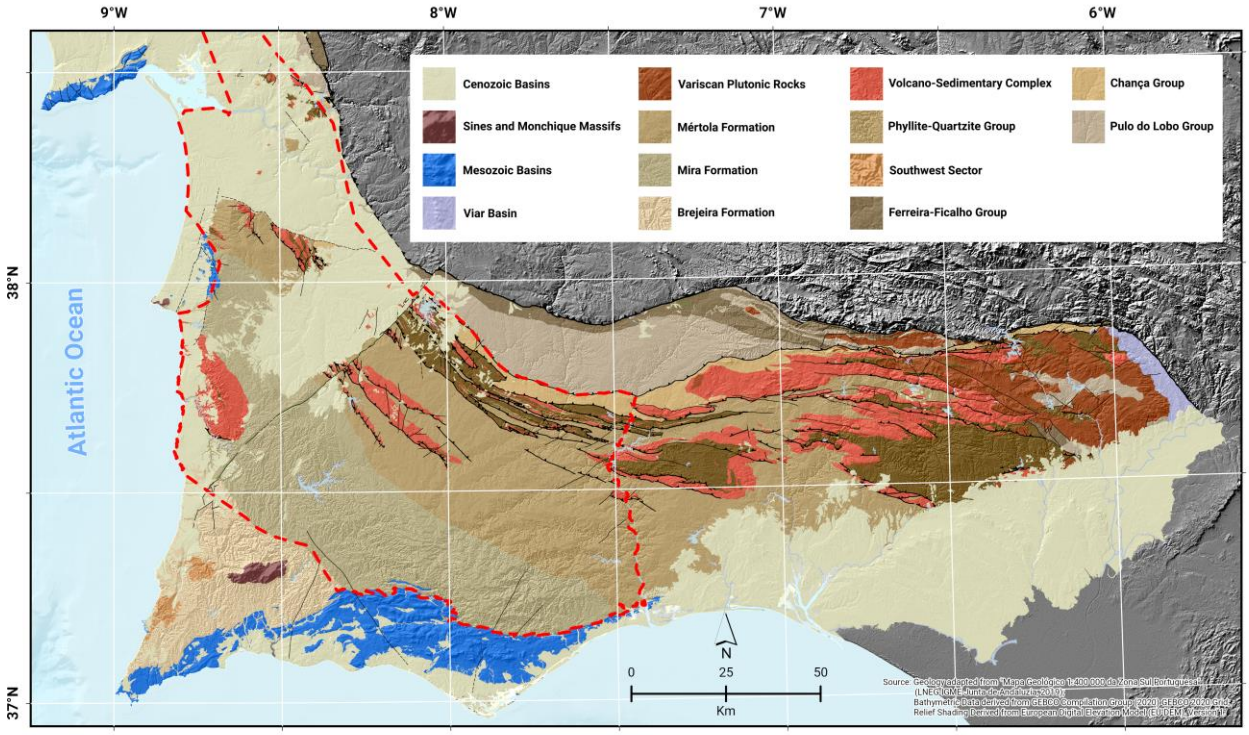

Figure 1. Simplified geological map of the IPB with the delineation of the Portuguese Sector of the Iberian Pyrite Belt (red dashed otted line).

Figura 1. Enquadramento geológico simplificado. Delineação do Sector Português da Faixa Piritosa Ibérica (tracejado vermelho).

Table 1*. Characteristics of multispectral remote sensing datasets.

Tabela 1*. Características dos dados multiespetrais de deteção remota.

Sensors and timeline	Bands	Centre Wavelength (nm)	Bandwidth (nm)	GSD** (m)
LANDSATETM+ 04/08/2000	1	485	70	30
	2	560	80	
	3	660	60	
	4	835	130	
	5	1650	20	
	6	11450	210	60
	7	2220	260	30
	8	710	380	15
QuickBird 07/11/2004	Panchromatic	729	648	0.6
	Blue	488	115	2.4
	Green	543	154	
	Red	650	120	
	Nir	817	203	
Sentinel 2 Ccaptured during the year 2017	1	442.7	21	60
	2	492.4	66	10
	3	559.8	36	
	4	664.6	31	
	5	704.1	15	20
	6	740.5	15	
	7	782.8	20	
	8	832.8	106	10
	8[a]	864.7	21	20
	9	945.1	20	60
	10	1373.5	31	
	11	1613.7	91	20
	12	2202.4	175	

*Source:https://landsat.gsfc.nasa.gov/the-enhanced-thematic-mapper-plus/; https://www.euspaceimaging.com/wp-content/uploads/2018/06/QuickBird-DS-QB-Prod.pdf and https://sentinel.esa.int/web/sentinel/user-guides/sentinel-2-msi/resolutions

** Ground Sampling Distance GSD (m) meters, nanometers (nm).

et al., 2018). For the southern Portugal, Sentinel 2 has been processed with the purpose of geological enhancement including mineralogical indices and target detection of mining centres.

Further studies include radiometric data comparison with Sentinel 2 data (Quental *et al.*, 2018), which was collected in total gamma and expressed in Exposure Rate in a radiometric map at 1:500 000 scale (Batista *et al.*, 2013). These data were gathered through decades of multitemporal acquisition with portable SPP2 scintillometers, land and airborne surveys and the objetive is to support Sentinel 2 interpretation.

3.2. Hyperspectral

The S. Domingos mining area was flown twice with different hyperspectral (IS) sensors (Figs. 2 and 3) both with contemporary spectroradiometric field measurements for validation and acquisition of relevant materials´s spectral signatures (Quental *et al.*, 2002, 2011a, b). The fligths gathered datasets for environmental purposes, to assess mining contamination encompassing the area of exploitation, mining infrastructures, cementation tanks, sulphur factories and ore transportation pathway. Another objective was to test the monitoring component with another sensor focused on the Acid Mine Drainage (AMD). Details of airborne and field sensors of both fligths and field campaigns are in figure 3 and in table 2.

3.3. HyMap™

This whiskbroom sensor, owned by Hyvista Corporation (HVC), used a Dornier 228 aircraft operated by the Deutsches Zentrum für Luft und Raumfahrt (DLR) to acquire the data.

The fligthlines captured by this sensor on 21st August 2000 covered an area of 726 km^2 corresponding to 11 strips (Quental *et*

al., 2002), from which 8 have been partially selected for detailed study as shown by the area in figures 2 and 3. Aerial photographs were also captured for generation of the Digital Elevation Model (DEM). Soil, water, and rocks were collected in subtest areas and analysed for geochemistry, X-Ray diffraction and further modelling with images together with field data collection undertaken in the subtest areas (Quental *et al.*, 2002).

Table 2. Characteristics of hyperspectral sensors on data capture over S. Domingos. Source. (in Quental, 2011).

Tabela 2. Características dos sensores hiperespetrais que capturaram dados sobre S. Domingos. Fonte: (in Quental, 2011).

Sensors	Characteristics	VNIR-SWIR (437-2485nm)	
HYMAP™	Acquisition Year	2000	
	IFOV	2.5 mr & 2.0 mr along and across track	
	FOV	61.3 degrees (512 pixels)	
	GIFOV	4.3m	
	Swath Width	2.3 km at 5 m IFOV	
	SNR	500:1	
	Bit Depth	11-bits	
	Spectral Resolution	18nm (average)	
	Nº Bands	126	
	Sensor Type	Push Broom	
SPECIM EAGLE HAWK		**VNIR (393-988nm)**	**SWIR (962-2451nm)**
	Acquisition Year	2007	
	IFOV	0.075º	
	FOV	34.69º	23.78º
	GIFOV	2m	
	Swath Width	0.43*height	
	SNR	450:1	800:1
	Bit Depth	12	14
	Spectral Resolution	2.9 nm	8.5nm
	Nº Bands	252	237
	Sensor Type	Whisk Broom	

3.4. SPECIM EAGLE-HAWK

This pushbroom sensor, with two sensors (Tab. 2) used a Dornier 228 aircraft operated by the National Environment Research Council (NERC)/ARSF (Airborne Research and Survey Facility) on behalf of the British Geological Survey (BGS) to acquire data over the S. Domingos area in March 2007 (Figs. 2 and 3). The average height of data capture was 1690 m at an average velocity of 267 km/h. Simultaneously a dataset collection took place (Quental *et. al.*, 2011b) for spectral measurements of calibration targets (Fig. 3) as well as selected potential contaminated materials related to AMD, and for further analysis. To further improve the accuracy and geometric precision of flight data, a field GNSS survey was conducted.

4. Methodology

The methodology employed to process remote sensed data was very specific to each dataset and tailored to the objectives of each project. Commonly *Environment for Visualizing Images* (ENVI, 2020) and the open source *Sentinels Application Platform* (SNAP; 2019) were used to pre-process and process the data and GIS software such as ArcGIS and QGIS used to map and display of the results.

4.1. Multispectral

For Landsat ETM+ multispectral data, an atmospheric correction was done using *Fast Line-of-sight Atmospheric Analysis of Spectral Hypercubes* (FLAASH) in ENVI software. Regarding Sentinel 2, there are two major data products – L1C and L2A. L1C corresponds to a Top-Of-Atmosphere (TOA) reflectance, orthorectified with sub-pixel multispectral registration and L2A to Bottom-Of-Atmosphere (BOA) reflectance (ESA, 2015). Most recent datasets of Sentinel 2 data are already available on level 2A, but when working with older datasets, data is only available at level 1C. To ensure the best possible results, when processing remote sensing data, atmospheric correction need to be performed (Main-Knorn *et al.*, 2017) and to process datasets from L1C to L2A, SNAP software was used with Sen2Cor plugin when needed specific granules. To generate a cloudless and seamless mosaic of the study area, to maintain spectral relationship between bands, reduced spatial noise, and consistency across scene boundaries (Roberts *et al.*, 2017), the platform Mosaic Hub was used. It provides an approach of pixel based composite mosaics which uses a decision tree approach as well several key components and criteria to evaluate and select the best information for a given pixel within a specific time series defined by the user (Roberts *et al.*, 2017). For the entire area, a mosaic was ordered in Mosaic Hub for the year 2017. The data received was divided in several granules, which was mosaiced band by band in SNAP, reprojected and resampled to the same spatial resolution (10 m) and then extracted the relevant information using a mask.

To increase the spatial resolution of the multispectral data Landsat ETM+ and QuickBird a Gram Schmidt Spectral Sharpening algorithm (GSSS) (Laben and Brower, 2000) was applied using Pan higher resolution and multispectral bands resulting in datasets respectively of 15.0m and 0.6m for all bands (Tab.1), while statistically maintaining the major spectral characteristics. Standard algorithms to extract information based on multivariate analysis i.e. Principal Components Analysis (PCA), Minimum Noise Fraction (MNF) and Independent Component Analysis (ICA), provide a new set of uncorrelated image bands retaining most of the variance (Girija and Mayappan, 2019). Classical classifiers, such as Spectral Angle Mapper (SAM) (Boardman and Kruse, 1994, Green *et al.*, 1988, Kruse *et al.*, 1993) were used together with enhancement tools using textural and mathematical morphology operators. The Landsat ETM+ had also another type of processing following the same methodology as described below in the same fashion of the hyperspectral images.

Specifically focused on geological information, geological indices were processed to highlight hydroxyl bearing alteration minerals (e.g. clays), ferrous iron oxides and all iron oxides (Drury, 1982, Segal 1987; Sabins, 1999). Wavelength ranges for Landsat ETM+, or equivalent for any multispectral images (Tab. 1), are respectively, for "clays" - band5/band7, "ferrous iron minerals" - band5/band4 and "iron oxides" - band3/band1. For Sentinel 2 the closest wavelengths (Tab. 2) are respectively band11/band12, for hydroxyl bearing alteration, all ferrous iron oxides band4/band11 and for all iron oxides band4/band2 (Van der Weerf *et al.*, 2016). These indices were also compared with radiometric data. A vegetation supression algorithm, available in ENVI (2020), was applied to remove the vegetation spectral signature using information from red and near-infrared bands.

4.2. Hyperspectral

Pre-processing in hyperspectral data HyMap™ included geocoding of fligthlines in UTM, WGS84 datum using

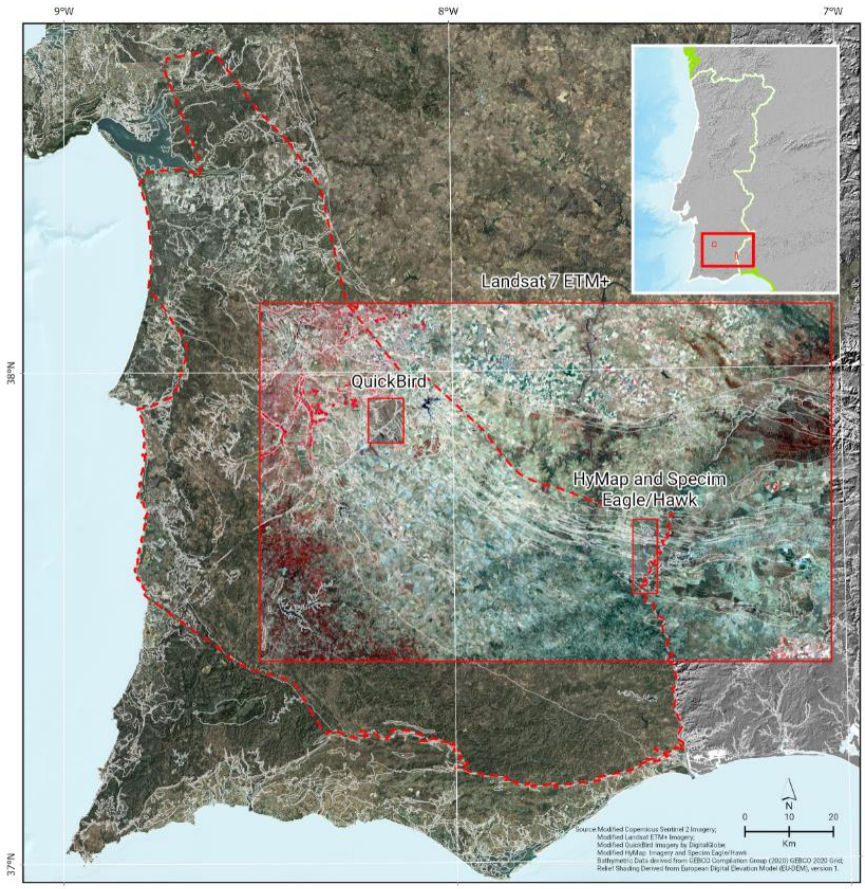

Figure 2. Overview of multispectral and hyperspectral remote sensing datasets overlayed on Sentinel 2 imagery and EU DEM. Timeline in tables 1 and 2. Red dashed line - delineation of the PSIPB. Geological limits adapted from 1: 400 000 South Portuguese Zone Geological Map (IGME-LNEG -Junta de Andaluzia, 2019).

Figura 2. Panorama dos dados multiespetrais e hiperespetrais sobrepostos ao mosaico do Sentinel 2 e EU DEM. Cronologia nas tabelas 1 e 2. Tracejado vermelho -delineação do SPFPI. Limites geológicos adaptados do Mapa Geológico 1:400 000 da Zona Sul Portuguesa (LNEG-IGME-Junta de Andaluzia, 2019).

Differential Global Positioning System (DGPS) flight data. The dataset was delivered by HVC as radiance and calibrated to reflectance data using HyCorr software (Quental *et al.*, 2002, 2011) (Fig. 3).

For the SPECIM EAGLE-HAWK, dataset was georeferenced using GPS data and other ancillary topographic data. Considering that the main purpose of the data capture was for Acid Mine Drainage (AMD) multi-temporal assessment using HyMap™ data captured in year 2000 (Quental *et al.*, 2002) the number of bands of the SPECIM EAGLE-HAWK was resampled as close as possible to the number of bands and wavelengths of the HyMap™ so was set to 124, excluding the last two that are not reached by SPECIM EAGLE HAWK (Tab. 2).

The data were mosaiced and the atmospheric correction undertaken using the FLAASH algorithm (Addler Brown, 1998), a module implemented in ENVI software. The atmospheric model selected is still considered a mid-summer latitude model, following temperature and latitude conditions as referred in Addler Brown (1998). The FLAASH algorithm operates on a pixel-by-pixel basis, taking advantage of the fact that each pixel in an imaging spectroscopy image contains an independent measurement of the atmospheric water vapour bands (differential absorption). An adjacency correction was considered. Local atmospheric conditions were provided by the nearest meteorological station (Beja airport). After correction, the mosaic was also polished using an Empirical Flat Field Optimal Reflectance Transformation™ (EFFORT) Polishing. The EFFORT method, as described by Goetz *et al.* (1997) and Boardman (1998), is an analytical process that bootstraps a linear adjustment to apparent reflectance spectra to improve the accuracy of spectra following calibration with ATREM. EFFORT. This has been done solely using image information and the three wavelength segments 437-1323 nm, 1433-1805 nm and 1970-2451 nm (Quental *et al.*, 2011b).

With significant diferences in the characteristics of the sensors (Tab. 2), to minimise the impact of different atmospheric corrections, a similar approach applied on the SPECIM EAGLE HAWK was undertaken to the HyMap™ radiance data.

The application of hyperspectral data for AMD and related pollutants detection has been mostly based on specific mineralogical mapping from spectral libraries or on field spectra derived information. For assessing mining contamination distincts approaches were undertaken (Quental *et al.*, 2011a, 2013): 1) based on field spectroradiometric measurements; and 2) multi-source spectral data for AMD mineralogical mapping. In 1) chemical analysis and X-Ray diffraction allows categorisation of hazardousness of the materials measured by spectroradiometers.

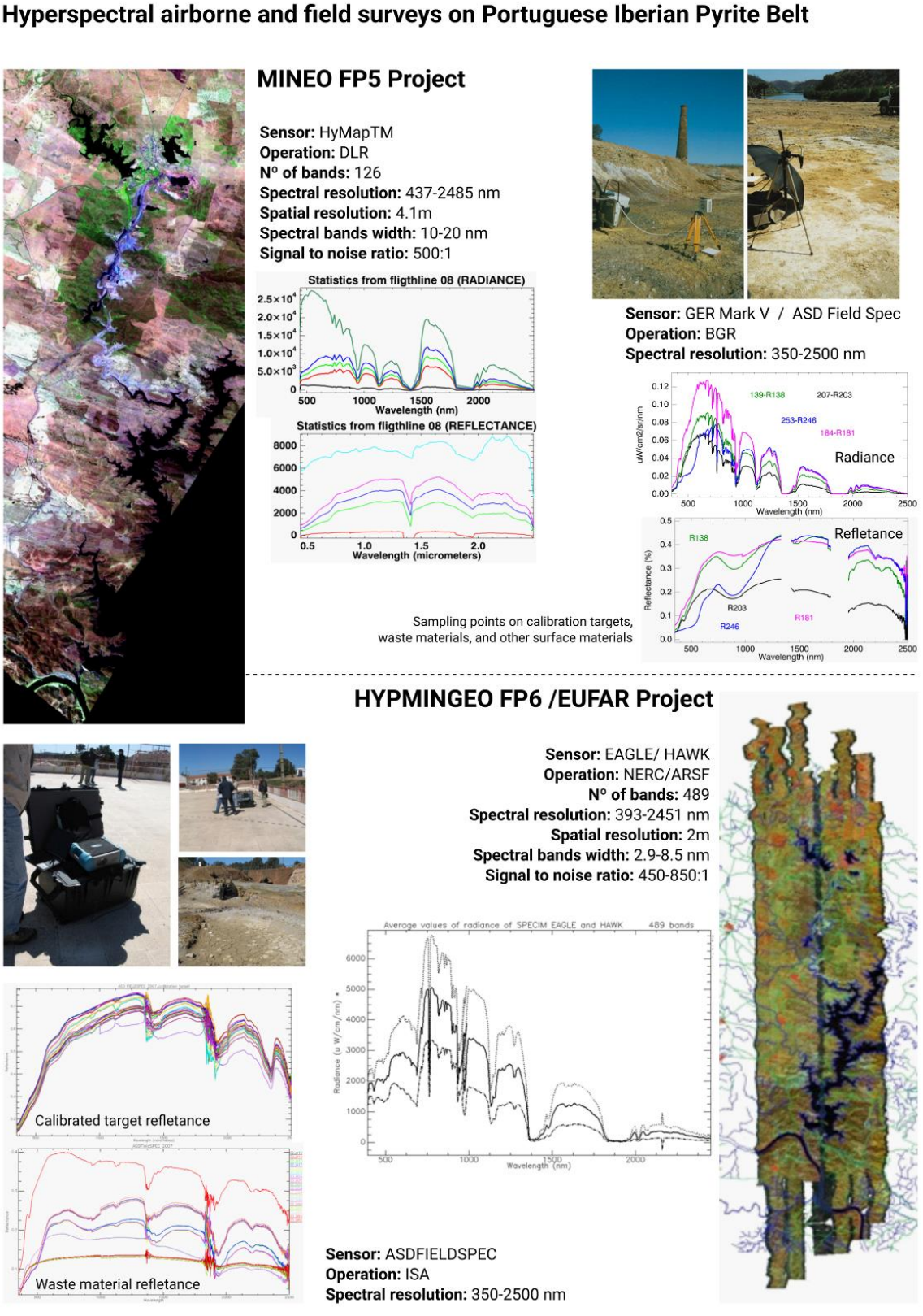

Figure 3. Hyperspectral airborne data capture and spectroradiometric field measurements for calibration and targets: Top - HyMap^{TM} data capture on 21 of August 2000, bottom – Specim Eagle Hawk data capture on 21 March 2007 and Specim Eagle Hawk fligthlines with ancillary topographic data.

Figura 3. Captura de dados hiperespectrais aerotransportados e medições espectroradiométricas: Topo HyMap^{TM} capturado a 21 de agosto de 2000, Base – Specim Eagle Hawk capturado a 21 de março 2007 e respetivas linhas de voo e dados -auxiliares topográficos.

The SAM algorithm was selected for generation of a waste mining materials map. A SAM algorithm (Kruse et al., 1993) is a physically based spectral classification that uses an n-dimensional angle to match pixels to reference spectra, treating them as vectors in the space with dimensionality equal to the number of bands. The methodology developed to minimise uncertainty in 2) uses as input data a) field spectral measurements, b) standard mineralogical spectral libraries (USGS) Clark et al., 2007), and c) endmembers derived from images following a sequential workflow (Quental et al., 2013). These three types of independent sources of spectral data are linked through a Pearson correlation matrix, which works as a spectra selector. Each of the unknown spectra is assigned to the USGS spectral library minerals. The high-level correlation of interest, ≥ 0.9, are then used as input for mapping the area using the SAM algorithm. The same methodology was also tested and utilized for the 2007 campaign (airborne and spectral measurements).

5. Results and discussion

5.1. Multispectral

A high-resolution land cover map for the Aljustrel mining area was derived from QuickBird images (Fig. 2), rescaling and updating the Corine Land Cover (CLC) map. This allowed the definition of the spatial distribute on patterns and perception of elements at risk. Other elements for characterisation included a vegetation index. Land cover characterization was based on level III of CLC2000 (Bossard et al., 2000), establishing the quantitative characterization of a potential contaminated area in case of dam failure (Quental, 2006, Quental and Matos, 2006). A detailed geological and mining map (Matos, 2006) was done based on the QuickBird image (Fig. 4). For the Sentinel 2 mosaic, a Principal Components Analyis (Gupta et al., 2013) was performed to compress the information available on the spectral bands. (Fig. 5). The three components C1C2C3 explain 99.20% of the overall variance of the image. These components mainly split the PSIPB area according to the units and formations as in figure 1, with some variations in the SE of the Mértola Formation.

The geological indices of mineral groups, highlight hydroxyl bearing alteration (e.g. clays) minerals, ferrous iron oxides and all iron oxides, ferrous oxides minerals, and all iron oxides (Segal 1982, Drury, 1987, Sabins, 1999), defined as band ratios, are displayed in figure 6 The group of "Clay Minerals" highlights hydrothermally altered rocks containing clay and alunite, Ferrous Minerals highlights iron-bearing minerals, and Iron Oxide (to oxidation of iron-bearing sulphides. Within the PSIPB, clay minerals from alteration of white detrital mica (Matos et al., 2020) are dominant in the Mira Formation with greywackes, siltstone and pelites, while Mértola Formation is a mixture of iron oxides and ferrous minerals with the dominance of the latter. Both formations are included in the Baixo Alentejo Flysch Group (BAFG, Oliveira et al., 2013).

This type of indices provides clues to be analysed together with other data for a valid interpretation. It must be considered the pattern designed superficially, whether vegetation or fire scars (blue areas in Mira and Brejeira formations in figure 6) are representatives and the interference with the exclusive geological signature. Among others, a relevant datatset for geological information and exploration issues is the radiometric map 1: 500 000 scale (Batista et al., 2013) and PSIPB 1:400 000 map Exposure Rate Total Count (Batista et al., 2016; Matos et al., 2020). In the domain of gamma rays (γ), far apart of the wavelength range of Sentinel 2, 443–2190 nm, this map was correlated with the processed Sentinel 2 mosaic images with the main geological and tectonic units mapped in the regional 1:200 000 geological map (SGP, Sheets 7 and 8) and 1:400 000 South Portuguese Zone (SPZ) Geological Map (IGME-LNEG -Junta de Andaluzia, 2019), as the main Meso-Cenozoic borders in the West and SPZ Paleozoic basement (Fig. 1). The geological limits of the Baixo Alentejo Flysch Group are well defined, e.g. boundaries of the Mira Formation (NE: Mértola Formation; SW: Brejeira Formation) (Figs. 1 and 7).

The geology of south of Portugal is well reflected in the radiometric map (Exposure Rate) in all geological domains of South Portuguese Zone: Pulo do Lobo, IPB, BAFG and SW Sector. In the Mesozoic sequences and Baixo Tejo/Alvalade Cenozoic Basin the results are also quite consistent. The Mira Formation high background related with common white K rich mica (muscovite/sericite) in the shale, greywacke and quartzwacke matrix allows a good contrast with the BAFG Mértola Formation and with the Brejeira Formation (Matos et al., 2020). Considering the homogeneous characteristics of these flysch sequences, radiometry is a good mapping support based on the differences of lithological/mineral composition.

Comparison with multispectral images, radiometry increases explanations of the remote sensing images and is well correlated with it. Specifically concerning Sentinel 2 dedicated geological indices, the processed mosaic gives important information about iron oxides, ferrous iron, and clay content. Compared with the radiometric signature, the marine sediments of the Mira and Brejeira formations show strong radiometric signatures, corresponding to the K content in clays, using both radiometric and satellite images.

Both radiometric data and Sentinel 2 processed images highlight the main convergence of geological information in southern Portugal. When divergent, the Sentinel 2 data adds clues for further investigation and analysis, capable to differentiate geological environments with dedicated image processing and highlight among IPB geology especially important areas of known mineral potential (Quental et al.,2018).

The uselfulness of combining radiometric data with image processing results can also be depicted when computing an Independent *Component Analysis*. (Girija and Mayappan, 2019) These components add more information for interpretability of geological patterns when analysed jointly with the radiometry map in a sector of the Mértola Formation in figure 8. It highlights the pattern of VS Complex and PQ Group otherwise indistinguishable in a natural image.

The combination of different layers derived from remote sensing improves the knowledge about the area, overlaying different datatsets (Fig. 9).

5.2. Hyperspectral

The mapping of mining waste materials on HyMap™ image using field spectroradiometric measurements and a SAM algorithm, showing the spatial pattern depicted by the dispersion on the area of exploitation, mining infrastructures, cementation tanks, sulphur factories and ore transportation routes (Quental *et al.*, 2011) is in figure 10. The most relevant field spectra used are compared in with average results of equivalent image class (Fig. 10). The statistical parameter coefficient of variation (CV), ratio of the standard deviation to the mean, is useful for comparing the degree of variation from one data series to another. Generally, a value of $CV < 1$ indicates low data variability and probably the absence of anomalous data, which is verified in these

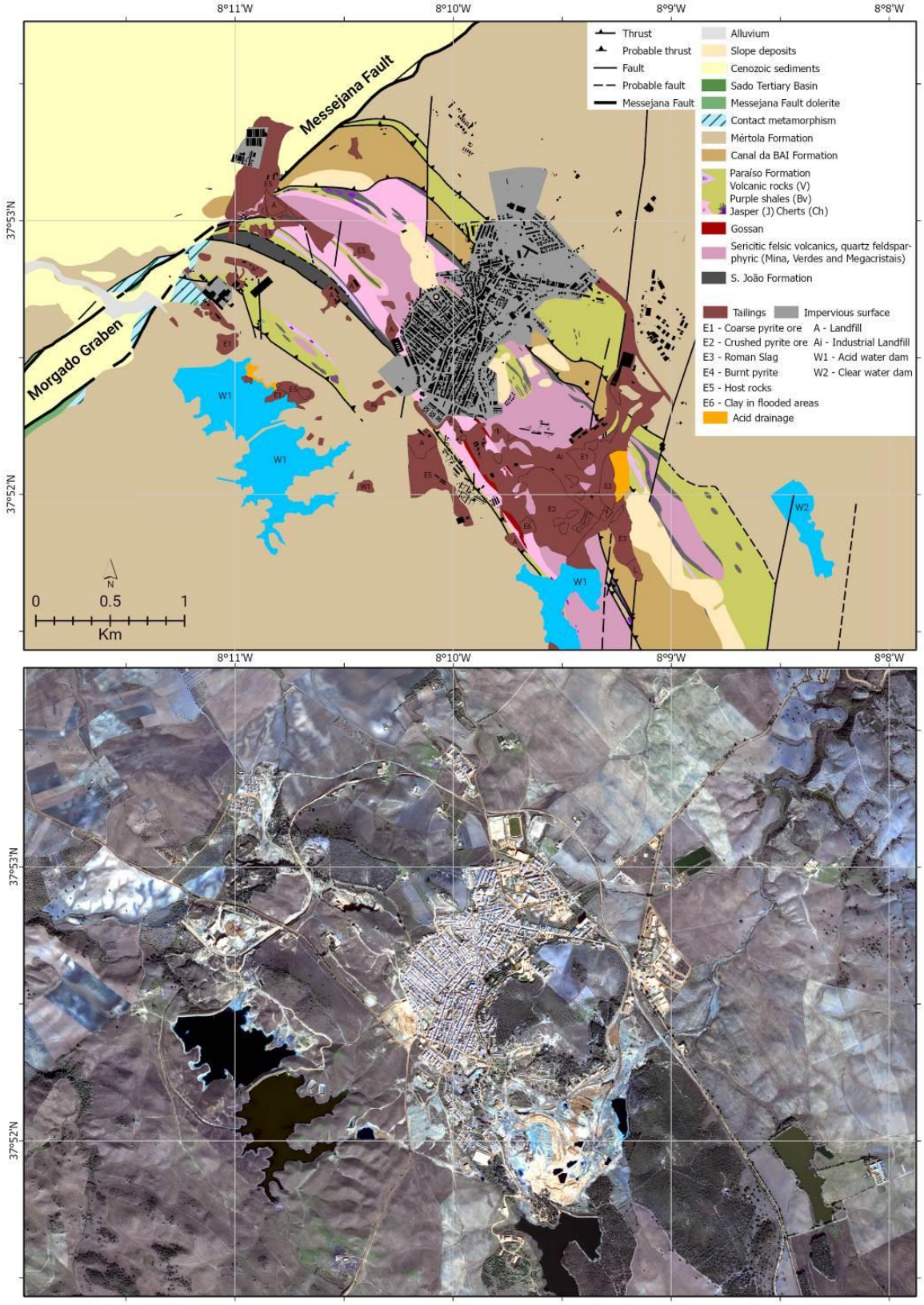

Figure 4. Geological and mining map of Aljustrel (adapted from Matos, 2006) and source natural RGB QuickBird image processed for 0.6m resolution. QuickBird © 2020 DigitalGlobe Inc., a Maxar Company.

Figura 4. Mapa geológico e de infraestruturas mineiras de Aljustrel (adaptado de Matos 2006) e imagem de origem QuickBird RGB natural processada para 0,6m de resolução. QuickBird © 2020 DigitalGlobe Inc., a Maxar Company.

classification results with an average CV of 0.29. The classes are also compared with other data type, namely waste field map, and mineralogy determined from XRD diffraction of soils clay fraction. The most relevant class for the AMD detection is the *mixed sulphur materials*, with visible native S within the samples measured. In fact, the total S content is commonly used in the prediction of acid production from mine wastes calculated in a static test of acid-base accounting (Levitan *et al*., 2007). The total S content reaches values of 7.93 mg g^{-1} in waste materials sampled at one of the test sites, Achada do Gamo, whilst the average values of 34 samples is 1.34 mg g^{-1} (Quental *et al*., 2002; Tavares *et al*., 2008).

The designation *contaminated* on two of the classes reports to the fact that geochemical analysis of the materials measured indicates high content of As, Hg, Pb, Sb and S (Tavares *et al*., 2008, 2009). However, some caution must be taken when extending the spectra "*contaminated soils and sediments",* from geochemical content of the samples, to the image scale. Although pollutant content is assigned to the spectra based on geochemical content of the sampled material, the extrapolation to a wide area remains with a certain degree of uncertainty. Particularly in this case, subtle differences in chemical composition might not be detected or differentiated using a SAM algorithm.

The results of the multi-source spectral methodology, that is also multi-scale by airborne, field measurements and standard spectral libraries are depicted in figure 12. The mineralogical correlation map ≥ 0.9 related to AMD shows assemblages of copiapite (Co) and coquimbite (Cq) typical of pH < 3 and surrounding very acidic ponds.

It is worth noticing the dispersion observed along the ore transporation routes. When not isolated, this class is followed spatially by jarosite, accompanied at lower but similar correlation levels, by minerals that indicate some information concerning higher pH values, such as goethite, schwertmannite or lepidocrocite.

The multi-source correlation matrix that assigns USGS (2007) standard mineralogical spectral libraries to unknown spectra allows another level of knowledge based on quantitative information. Thus, the wide variability within apparently similar and nearby sampling points as detected on field spectra, is only clarified by the quantitative assessment through the correlation matrix. This is confirmed by the multi-source spectral mapping, where the assignment of mineralogical spectra to unknown field spectra allows the establishment of correlation levels for the retrieval of information with improved knowledge and precision about the spectra considered (Quental *et al*., 2011a). This kind of information is advantageous, when correlating field and mineralogical library spectra based on wavelength values. In fact, the high precision information derived from spectral data requires a different type of approach and the establishment of a quantitative link works well to retrieve information of the spectra otherwise impossible just by visual analysis of absorption features and forms (Figs. 10 and 11). An important and relevant point is that low pH *copiapite-coquimbite* at correlation ≥ 0.9 is never with minerals other than alunite. At lower correlation level these minerals are associated with illite, kaolinite or smectite. Lower values of correlation, i.e., < 0.8 do not depict different minerals exceptionally if below 0.5 quartz, a-jarosite or pyrite This indicates the significance of these mineralogical assemblages by isolation at high correlation level.

The comparison of the two maps, AMD waste mining materials and AMD mineralogical correlation depicts the improvement given by a multi-source spectral methodology, by isolating copiapite (coquimbite) (alunite) as mineralogical assemblages of low pH at correlations above 0.9. It also provides accuracy on the mapping results and improved knowledge about the mineralogical assemblages related to AMD.

It is worth noticing that these two types of maps, waste mining materials and AMD mineralogical correlation map of hyperspectral datasets, have been translated into the contemporary Landsat ETM+ (Tab. 1) following specific procedures for degrading to the wavelength range of the multispectral resolution. The results generating a similar map of pH < 3 opens perspectives for the routine use of spaceborne multispectral data, but with less uncertainty relying on input of hyperspectral knowledge into multispectral processing (Quental, 2011) In 2007 hyperspectral dataset, the multi-source correlation methodology had a lack of significant spectral information concerning extraction of endmembers. These difficulties could be due to spectra spiking and faulty channels, with a potential partial contribution when spectrally subsetting the SPECIM EAGLE HAWK to the nearest HyMap™ characteristics (Tab. 2) (Quental, 2011). The different swath widths of the two sensors EAGLE and HAWK, the windy conditions of data capture including a failure of the sensor in the central fligthline (Fig. 2), led to the loss of some areas of the SWIR channel, in which were one of the calibration targets (Tab. 2, Fig. 2). A partial methodology was applied, excluding the independent source of endmembers derived from aiborne data. The correlation matrix using the field spectral measurement (n = 85) assigned to the USGS (2007) mineralogical spectral library are depicted in figure 12. As in 2000 field spectral data, apparent similar spectra depict distinct content when analysing the results of the Pearson correlation matrix, providing more information about the mineralogical assemblages. The spectra were selected at a correlation level > 0.8. for mapping 2007 SPECIM EAGLE HAWK fligth dataset and focused on signatures of low pH. The results mapped dominantely an area of figure 13, encompassing the open pit (D. Domingos) and downstream acidic dam and a sulphidic ore stockpile between the two, the two classes related to AMD gives a copiapite-(Coquimbite) alunite class in an area of 1,378.420 m² and a jarosite class with 2,286.160 m² (Quental et al., 2011b). Applying the same spectra to the HyMap™ 2000 mosaic, with the same atmospheric correction the results depict a much broader area related to the pH < 3 class copiapite-coquimbite minerals, compatible with the wider pattern depicted by the presence of efflorescent salts (Fig. 12, lower right photo) during summer. However, the mapped areas cannot be addressed in a quantitative way but merely as an evolutionary trend, due to the differences established in both mosaics (Tab. 2), adding to this the typical co-registration issues of the flights, as visible in figure 13.

The comparison of average reflectance of hyperspectral datasets, 2000 and 2007, show some changes in the global average spectral pattern, part of this related to seasonal variation, evidenced by the "red edge" feature. Other significant changes report to flattened average spectral response from HyMap™ of year 2000, compared with absorptions features clearly defined on SPECIM EAGLE HAWK of year 2007, i.e. at 492, 599, 678, 985, 1138, 1163, 1990 and 2028 nm. Generally, in the segments 1433-1805 nm there is a shift of the broader shape to the higher wavelengths of 2007 average values, while in the segment 2028-2485 nm the reflectance values increase from 2000 to 2007 datasets. In a more detailed scale, comparing local targets with field spectra gathered simultaneously with the sensor, as well as with hyperspectral 2000 data, there are differences in which are not completely clear the reasons. This include but are not limited to, the seasonality corresponding to the wet period of the S. Domingos area in 2007 comparing to the dry period in 2000 and

consequent effects on the vegetation patterns, and the different viewing angle and illumination geometry (Quental, 2011).

Given that the multi-source correlation methodology had a lack of significant spectral information concerning extraction of endmembers from SPECIM EAGLE HAWK, and thus missing one of the components for decreasing uncertainty, no further developments were undertaken concerning multispectral contemporary data, *e.g.* Landsat.

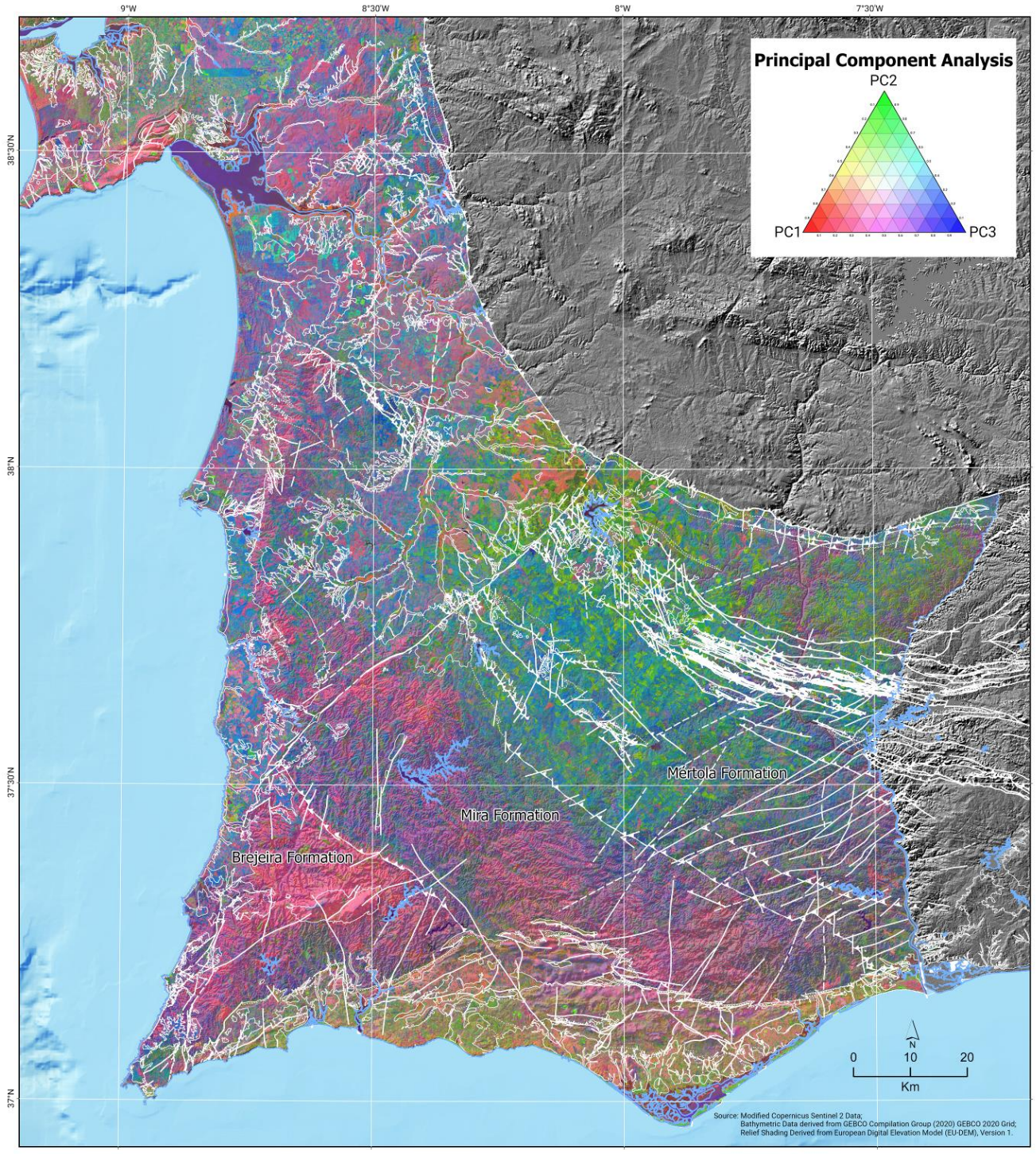

Figure 5 Principal Component Analysis on Sentinel 2 Mosaic. RGB Channels: 123.Portuguese Sector of the Iberian Pyrite Belt.

Figura 5. Análise de Componentes Principais no mosaico Sentinel 2. Canais RGB: 123. Setor Português da Faixa Piritosa Ibérica.

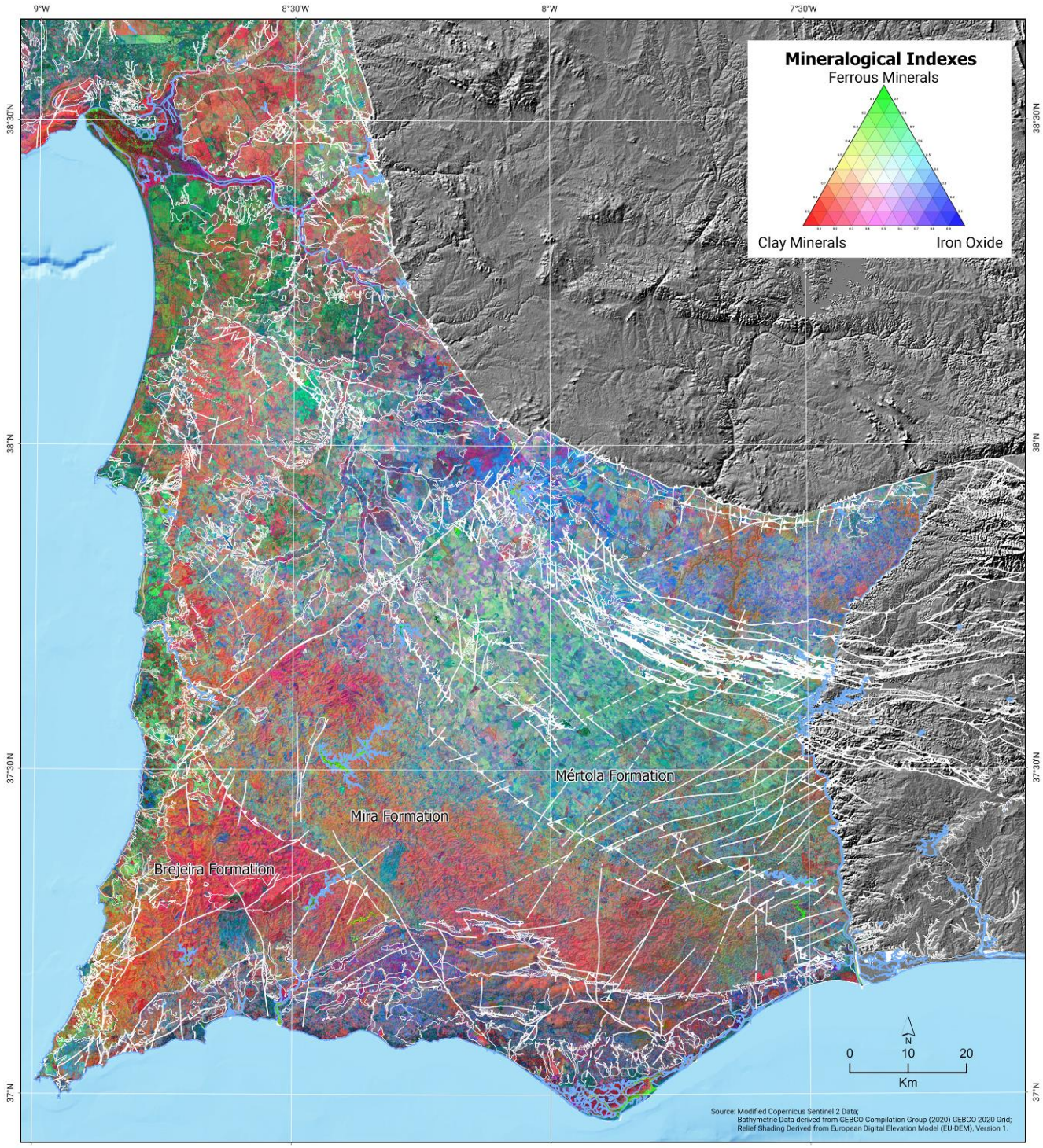

Figure 6. Spatial pattern of hydroxyl bearing minerals, ferrous iron minerals and iron oxides minerals after Segal (1982), Drury (1987) and Sabins (1999) Processed on Sentinel 2 Mosaic.

Figura 6. Distribuição espacial de minerais com hidróxilos, minerais com ferro ferroso e minerais de óxidos de ferro segundo Segal (1982), Drury (1987) e Sabins (1999) processados com base no mosaico Sentinel 2.

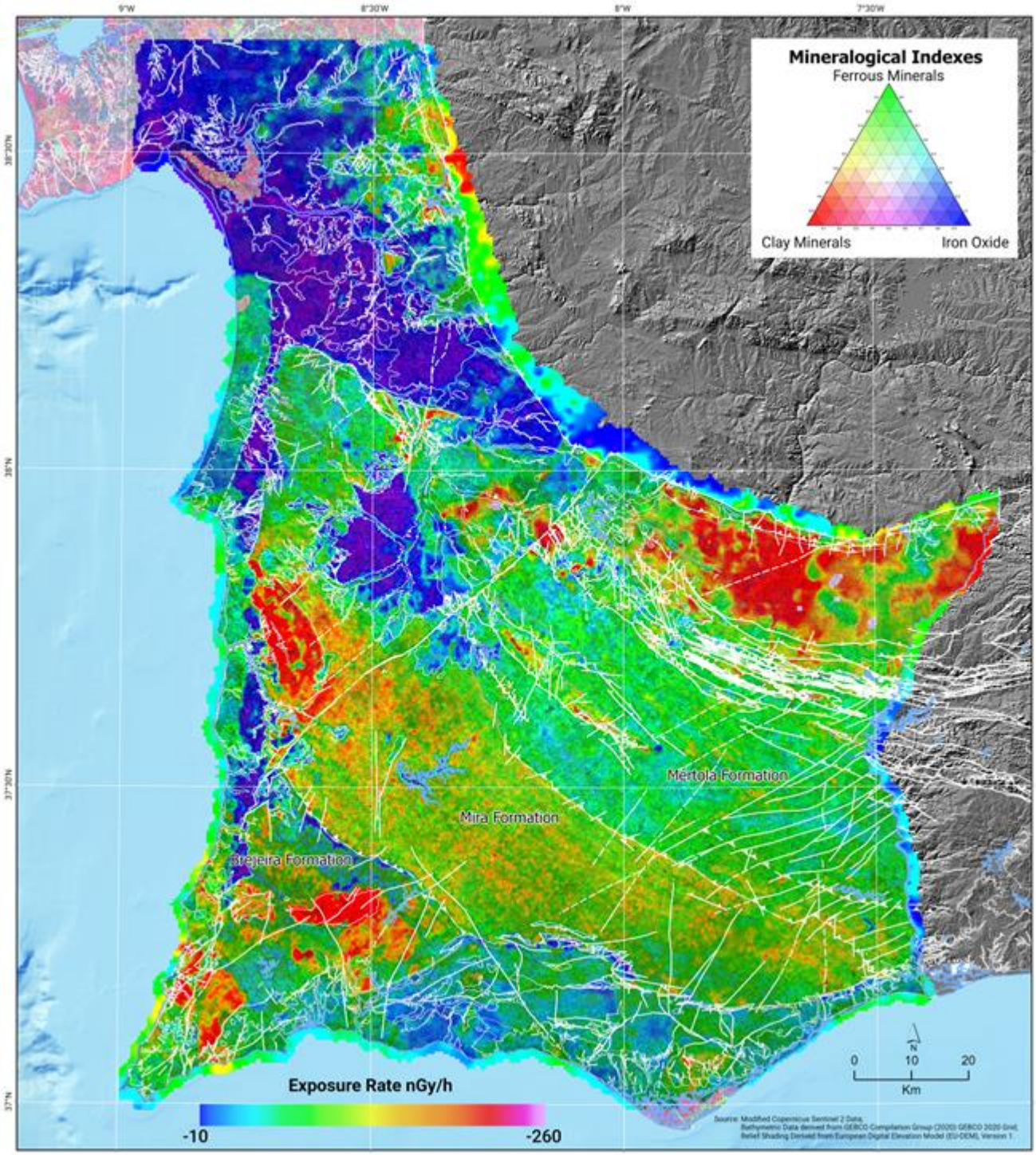

Figure 7. Combined visualizon of minerals indices of figure 6 and radiometry map 1:500 000 (Batista *et al.*, 2013).

Figura 7. Visualização conjunta dos indices mineralógicos da figura 6 e mapa radiométrico 1:500 000 (Batista *et al.*, 2013).

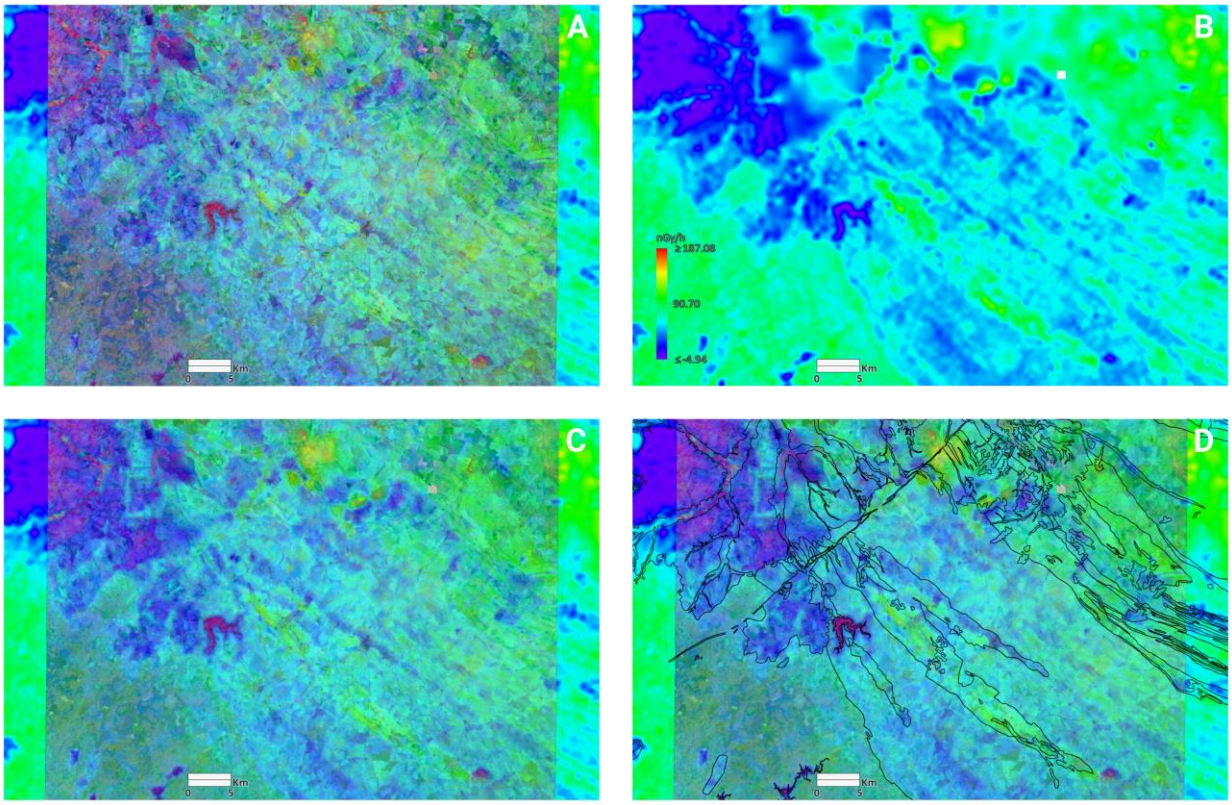

Figure 8., Independent Component Analysis (ICA) processed on Sentinel 2 mosaic and relationship with radiometry map (Batista *et al*., 2013): (A)- RGB: C5C2C3 – for a sector of Mértola formation where is seen the continuity with the underlying radiometry map, the radiometry map solely (B), with 50% transparency A and B (C), and the same as C overlayed with geology limits (D).

Figura 8. Análise de Componentes Independentes (ACI) processados no mosaico Sentinel 2 e relação com o mapa radiométrico (Batista *et al*., 2013): (A) - RGB: C5C2C3 para um sector da Formação de Mértola vendo-se a continuidade com o mapa radiométrico subjacente, o mapa radiométrico isolado (B), com 50% transparência A e B (C), idêntico a C e com os limites geológicos sobrepostos (D).

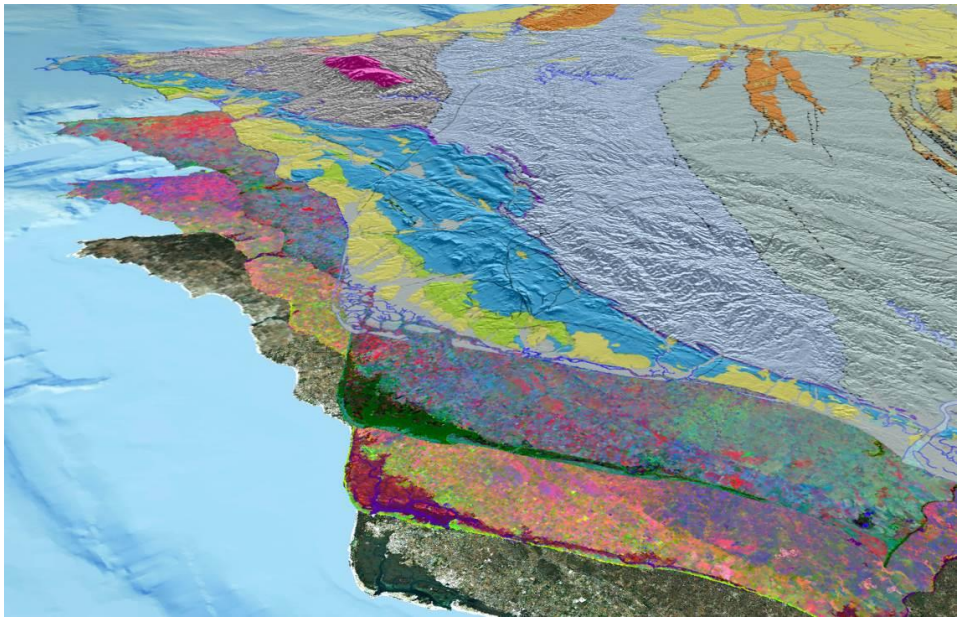

Figure 9. Model with layers of information seen from SSE to NNE top down: geology overlayed on EU DEM, Principal Components Analysis, PCAgeological indices and RGB natural composite 432.

Figura 9. Modelo com layers de informação vistos de SSE para NNW, de topo para baixo: geologia sobreimposta ao EU DEM, Análise de Componentes Principais ACP, indíces geológicos e imagem compósita natural RGB: 432

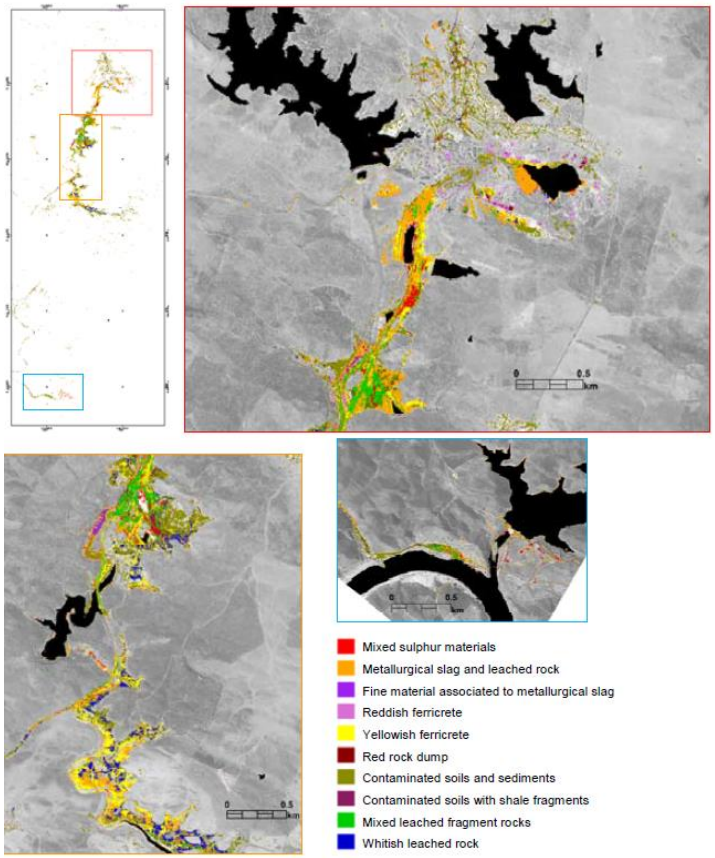

.

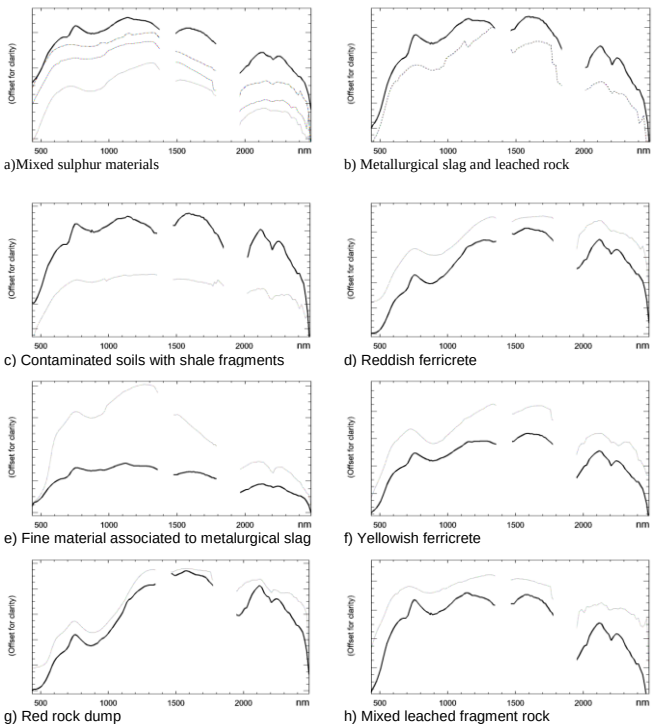

Figure 10. Map of Acid Mine Drainage waste materials based on field spectra and using Spectral Angle Mapper (adapted after Quental *et al.*, 2011) Upper left: scheme of the detailed maps and general framework in figure 2. Spectral signatures of the main classes (solid dark line) with field spectra (dotted light).

Figura 10. Mapa de Drenagem Ácida de materiais mineiros baseado em espectros de campo e utilizando o Mapeamento de Ângulo Espetral. (adapatdo de Quental *et al.*, 2011). Campo superior esquerdo: esquema dos mapas detalhados e enquadramento geral na figura 2. Assinaturas espetrais das classes principais (linha sólida escura).

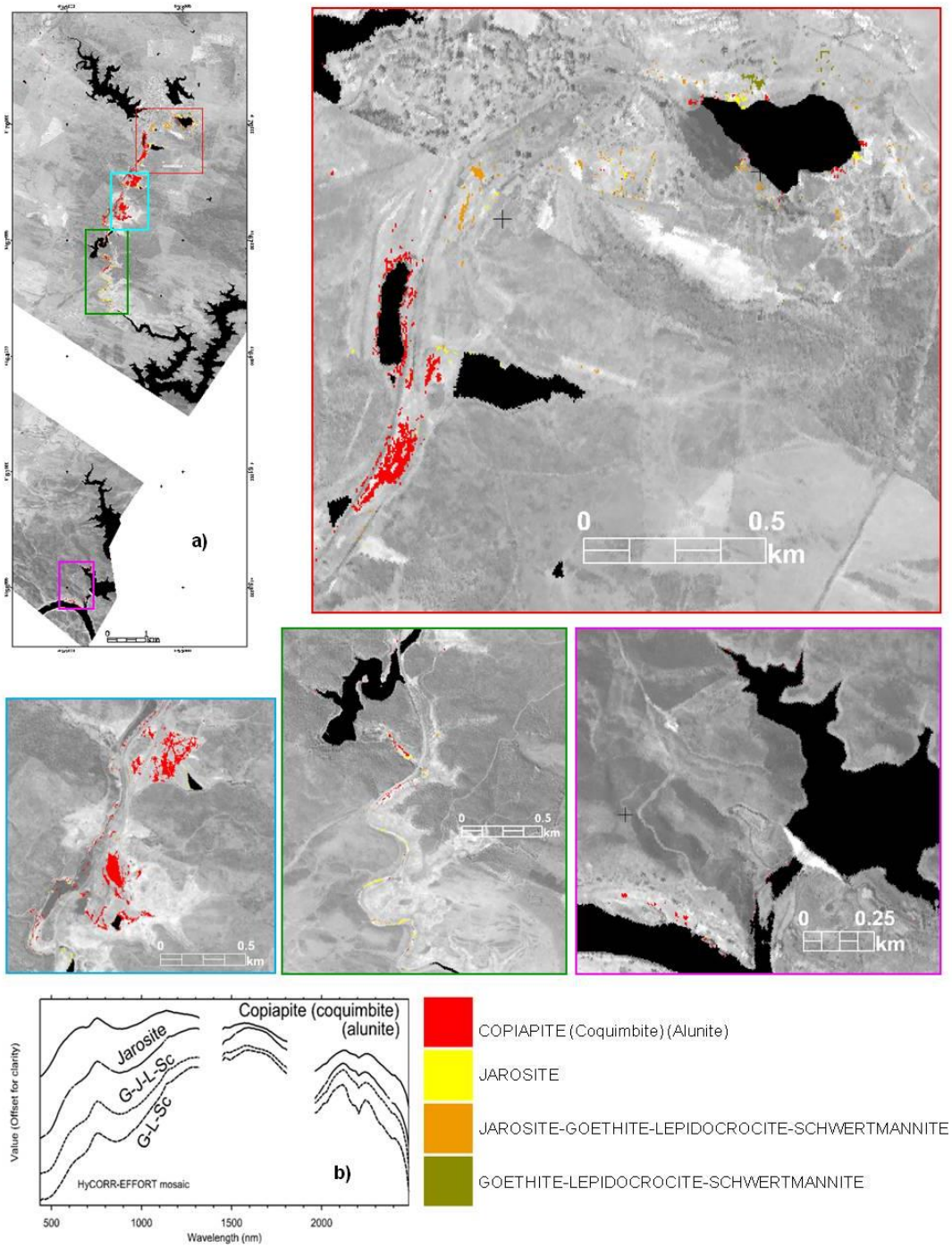

Figure 11. Mineralogical correlation map ≥ 0.9 related to Acid Mine Drainage. Assemblages of copiapite-coquimbite are typical of pH < 3. Upper left: scheme of the detailed maps; b) Average values of spectra of the classes, lower left (after Quental *et al* 2011).

Figura 11. Mapa de correlação mineralógica ≥ 0.9 associado à DAM. Associações de copiapite-coquimbite são típicas de pH < 3. Campo superior esquerdo: esquema dos mapas detalhados; b) Valores médios dos espectros das classes, campo inferior esquerdo. (adaptado Quental *et al* 2011a).

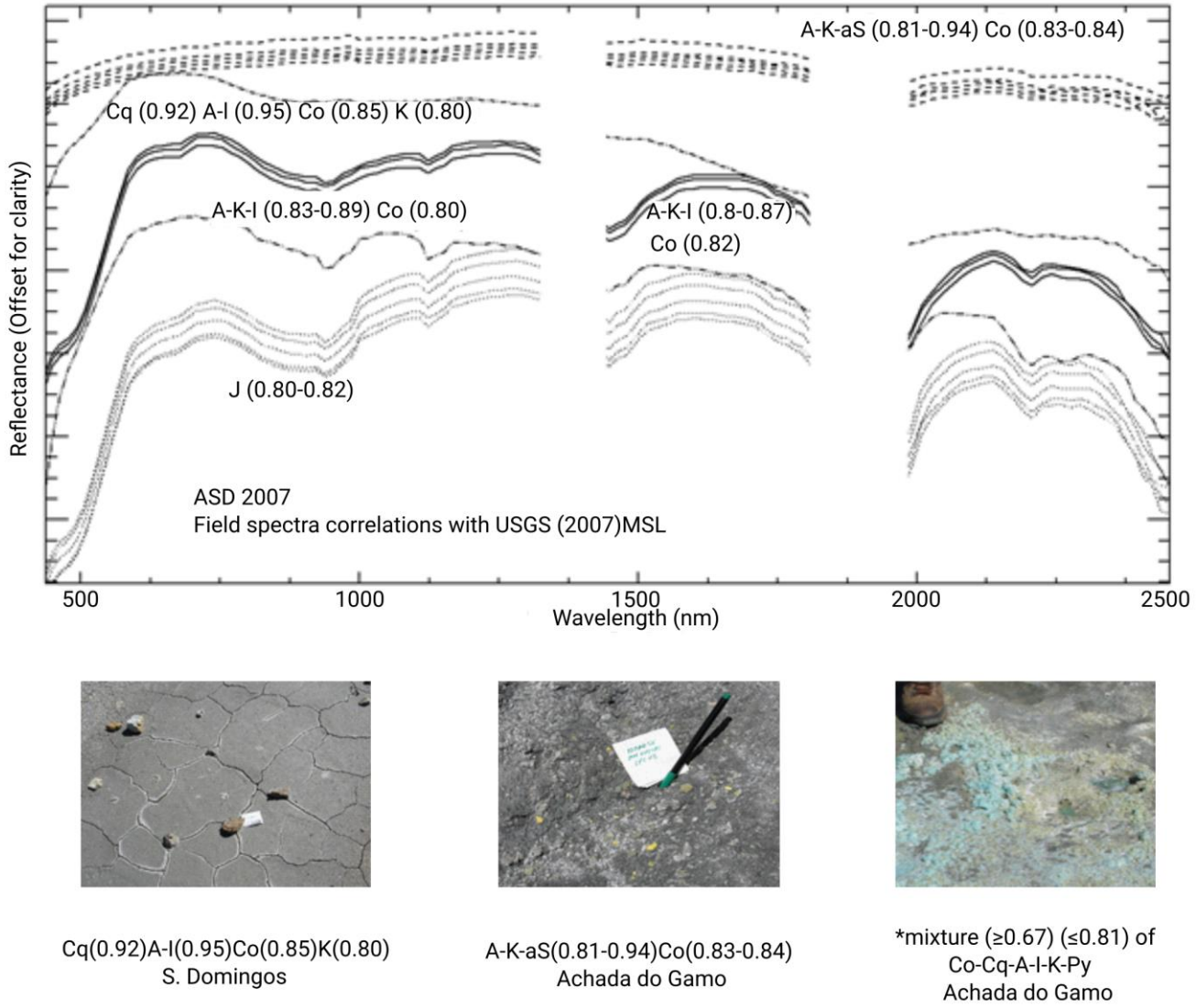

Figure 12. Upper - Spectral patterns from field data (n=85) acquired in 2007 and information derived from the correlation matrix with the USGS (2007) mineralogical spectral library. J-jarosite, Co-copiapite, Cq-coquimbite, aS-a-smectite, I-Illite K-kaolinite, A-alunite and Py-pirite. Lower - materials in which measurements were obtained, *not captured at image level (Quental, 2011).

Figura 12. Topo - padrão espetral dos dados de campo (n=85) adquiridos em 2007 e informação derivada da matrix de correlação com a biblioteca espetral USGS 2007. J-jarosite, Co-copiapite, Cq-coquimbite, aS-a-esmectite, I-Illite K-caolinite, A-alunite e Py-pirite. Base - materiais medidos, *não capturado ao nível da imagem (Quental, 2011).

6. Final remarks

Throughout the two decades of research on spectral information, derived from spaceborne, airborne sensors or field data, has contributed for incrementing knowledge in the PSIPB, either for geological or mining related purposes. This is valid for multispectral data, Landsat and Sentinel 2, including high spatial resolution QuickBird, or hyperspectral, high spectral resolution, HyMap^{TM}, SPECIM EAGLE HAWK and ASD field spectroradiometers. This quantitative digital spectral support of information combined with other data sources, radiometry, geochemistry, and geology, provide a distinct and enhanced knowledge of the area. The importance of combining multiple sources of data, is valid both for multispectral as well as for hyperspectral data. In the latter, this has led to the development of a multi-source spectral methodology for minimizing uncertainty about mapping results, establishing a quantification of pH < 3 for AMD at high correlation level, ≥ 0.80 or ≥ 0.90 isolating specific mineral assemblages. The assignment of unknown spectra to the mineralogical content of standard spectral libraries (*e.g.* USGS, 2007) through a correlation matrix is an important achievement for more advanced knowledge of spectral information related to AMD behaviour. Further research is ongoing on this subject extending the tests to other thematic areas other than environmental concerns. The multi-source spectral methodology also highlights the importance of developing knowledge that decreases the uncertainty in mapping results.

The research developed highlighted the complexity of a multi-sensor approach, and limitations related to airborne data capture such as aircraft's ability to fly due to atmospheric and meteorological conditions, sensor availability and technical issues, among others. Part of these, can presently be surpassed by the use of unmanned aerial vehicles (UAV) allowing the fast and precise acquisition of very high-resolution data (Jakob et al. 2017) - temporal, spatial and radiometric. The ability to deploy the UAV on demand, is very important for data acquisition and constant monitoring of target sectors, also the increased

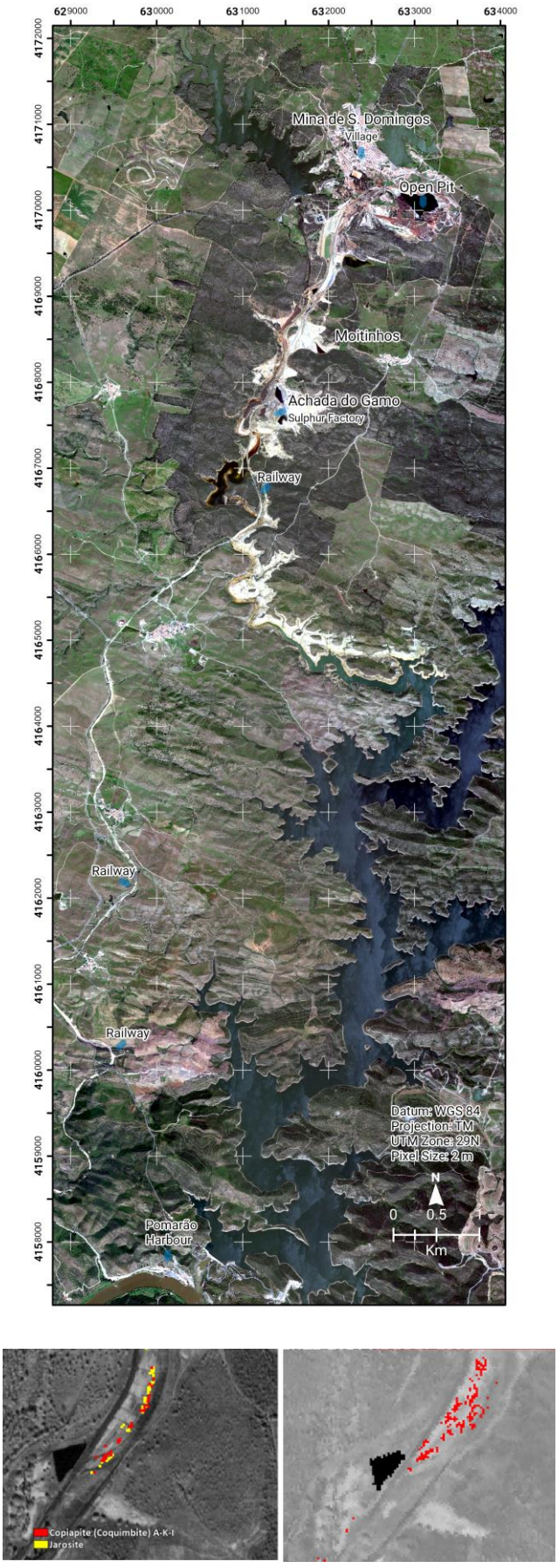

Figure 13. SPECIM EAGLE HAWK (RGB: 647, 554, 463 nm) and detail of dispersion of AMD between the open pit and Moitinhos: left: 2007 fligth, right 2000, both with 2007 field spectra (after Quental et al., 2011b; Quental, 2011).

Figura 13. SPECIM EAGLE HAWK (RGB: 647, 554, 463 nm) e detalhe de dispersão de AMD entre a corta a céu aberto e Moitinhos. Esquerda: voo de 2007, direita: voo de 2000, ambos com espetros de campo de 2007 (após Quental et al., 2011b; Quental, 2011).

availability of hardware, UAV and payloads, enables more detailed studies. In the field of applied geology, the use of different payloads enables the use of different techniques such as photogrammetry, lidar, multipectral, hyperspectral, thermal, and even magnetic and radiometric surveys (Park and Choi, 2020) enables more detailed works to be performed and overcome the scale gap between field and air-borne remote sensing, thus providing high-resolution and multi-temporal data on demand.

In the past years remote sensing observed some remarkable advances, from new multispectral and hyperspectral missions, and data availability, to improved software and methods to further process, generate products and analyse the data and results. Nevertheless, for passive optical sensors, cloud cover and land use/land cover (*e.g.* vegetation, burnt areas) may constrain the capacity to acquire information for the specific task proposed by the user.

Ongoing research within PSIPB includes the use of advanced image fusion algorithms (Ghassemian, 2016), to merge images with different radiometric and geometric characteristics, to generate new products and base knowledge, as a continuous improvement for this important sector.

Aknowledgements

Remote sensing works within the Portuguese Sector of Iberian Pyrite Belt were funded by several projects: MINEO *IST-1999-10337-5th FP*, e_EcoRisk *EVG1-2001-0087-5thFP*, HYPMINGEO-EUFAR 6th FP, EVALUSE POCTI/ECM/61699/2004. Recent research was supported by EXPLORA – Definition of new geological, geophysical and geochemical knowledge vectors applied to Neves-Corvo northern region, Op ALT20-03-0145-FEDER-000025, funded by Alentejo 2020, Portugal 2020 and European Union (ERDF) and GEO-FPI/Interreg POCTEP – Cross-border observatory for the geo-economic valorisation of Iberian Pyrite Belt, LNEG in association with Instituto Geologico y Minero de España, Junta de Andalucia and Câmara Municipal of Aljustrel.

L. Quental PhD grant (BD/17257/2004) was awarded by Foundation of Science and Technology. JMBC was supported by the Natural Environment Research Council (Agreement PR140015 between NERC and the National Centre for Earth Observation).

Thanks are also due to the Natural Environment Research Council (British Geological Survey), responsible for the airborne data captured in 2007, and to Mr. Andrew Wilson from AWK Technologies for the initial support in analysing the SPECIM-EAGLE Hawk data. Eng. Pedro Sousa was responsible for the setup of all GPS field data acquisition in 2000 and 2007, resolving several logistics and technical issues.

We are grateful to Professor José Cardoso Pereira who facilitated the use of the ASD field spectroradiometer owned by *Instituto Superior de Agronomia* in 2007 simultaneously with airborne survey. We acknowledge Copernicus the European Union's Earth Observation Programme, and the European Space Agency (ESA) for kindly providing the Sentinel-2 images. We used Copernicus Sentinel-2 data processed to level 2A by the French land data service center (Theia: https://www.theia-land.fr).

We are thankful to the Editorial Commission for the invitation to participate in this special edition, as well as permission to use the figures published in *Comunicações Geológicas* in 2011.

We thank Professor Pedro Pina whose comments and suggestions helped to improve and clarify this manuscript.

References

Adler-Golden, S. M., 1998. MODTRAN Cloud and Multiple Scattering Upgrades with Application to AVIRIS. *Remote Sens. Environ*., **65**: 367-375.

Almodóvar, G., Yesares, L., Sáez, R., Toscano, M., González, F., Pons, J. M., 2019. Massive Sulfide Ores in the Iberian Pyrite Belt: Mineralogical and Textural Evolution. *Minerals*, **9**, 653. Doi:10.3390/min9110653.

Barriga, F., Carvalho, D., Ribeiro, A., 1997. Introduction to the Iberian Pyrite Belt. *SEG Neves Field Conference. Guidebook Series*, **27**: 1-20.

Batista, M. J., Torres, L., Leote, J., Prazeres, C., Saraiva, J., Carvalho, J., 2013. *Carta Radiométrica de Portugal (1:500 000)*. https://geoportal.lneg.pt.

Batista, M. J., Torres, L., Leote, J., Prazeres, C., Saraiva, J., Carvalho, J., Matos, J. X., 2016. *Carta Radiométrica (Contagem Total) da Zona Sul Portuguesa, Faixa Piritosa Ibérica, esc. 1:400 000*. Edição LNEG/URMG, Lisboa, ISBN: 978-989-675-045-9.

Boardman, J. W. 1998. Post-ATREM Polishing of AVIRIS Apparent Reflectance Data Using EFFORT: A Lesson in Accuracy Versus Precision. *AVIRIS 1998 Proceedings, JPL, California*, 1998. http://Makalu.Jpl.Nasa.Gov/Docs/Workshops/98_Docs/7.Pdf

Bossard, M., Feranec, J., Otahel, J., 2000. *Corine land cover technical guide - Addendum 2000*. http:// terrestrial.eionet.europa.eu/. EEA Technical report No 40. Copenhagen (EEA).

Clark, R. N., Swayze, G. A., Wise, R., Livo, E., Hoefen, T., Kokaly, R., Sutley, S. J., 2007. *USGS Digital Spectral Library Splib06a*. U.S. Geological Survey, Digital Data Series 231, Http://Speclab.Cr.Usgs.Gov/Spectral.Lib06.

COM (2017) 490 final, 2017. *Communication from the commission to the European parliament, the council, the European economic and social committee and the committee of the regions on the 2017 list of Critical Raw Materials for the EU*. 8.

De Oliveira, D. P. S., Batista, M. J., Matos, J. X., Silva, T. P., 2020. Mineral sustainability of the Portuguese sector of the Iberian Pyrite Belt. *Comunicações Geológcas*, **107**(III): 11-20.

Digital Globe, 2019. *Quickbird Data Sheet*. Https://Dg-Cms-Uploads-Production.S3.Amazonaws.Com/Uploads/Document/File/100/Quickbird-DS-QB-Prod.Pdf. Accessed Online June 2020.

Drury, S. 1987. *Image Interpretation in Geology*. London: Allen and Unwin, 243.

ENVI, 2020. *Environment for Visualising Images*. Software Version 5.5.3, Harris Geospatial Solutions.

ESA (European Space Agency), 2015. Sentinel-2 User Handbook. *ESA Standard Document*, Issue 1, Revision 2, 24/07/2015, 64. Fal, S., Maanan, M., Baidder, L., Rhinane, H., 2019. The Contribution of Sentinel-2 Satellite Images for Geological Mapping in The South of Tafilalet Basin (Eastern Anti-Atlas, Morocco). *ISPRS - International Archives of The Photogrammetry, Remote Sensing and Spatial Information Sciences*. XLII-4/W12. 10.5194/Isprs-Archives-XLII-4-W12-75-2019.

Ghassemian, H., 2016. A review of remote sensing image fusion methods, Information Fusion. **32**(A): 75-89. ISSN 1566-2535, https://doi.org/10.1016/j.inffus.2016.03.003.

Girija, R. R., Mayappan, S., 2019. Mapping of Mineral Resources and Lithological Units: A Review of Remote Sensing Techniques. *International Journal of Image and Data Fusion*, **10**(2): 79-106. DOI: 10.1080/19479832.2019.1589585.

Gupta, R., Tiwari, R., Saini, V., Srivastava, N., 2013. A Simplified Approach for Interpreting Principal Component Images. *Advances in Remote Sensing*, **2**: 111-119. 10.4236/Ars.2013.22015.

Jakob, S.; Zimmermann, R.; Gloaguen, R. 2017. The Need for Accurate Geometric and Radiometric Corrections of Drone-Borne Hyperspectral Data for Mineral Exploration: MEPHySTo—A Toolbox for Pre-Processing Drone-Borne Hyperspectral Data. *Remote Sens*., **9**: 88.

Laben, C. A., and Bernard, V. B., 2000. *Process for Enhancing the Spatial Resolution of Multispectral Imagery using Pan-Sharpening*. US Patent 6,011,875, filed April 29, 1998, and issued January 4, 2000.

Levitan, D. M., Seal, R. R., Piatak, N. M., Hammarstrom, J. M., 2007. Evaluation of acid-generating potential of complex mine wastes. *Geological Society of America, Abstracts with Programs*, **39**(6): 404.

Locutura, J., 2011. Descripcion de las mineralizationes de sulfuros massivos de la Zona Sud Portuguesa. *In*: García-Cortés, A. (Ed.), *Cartografía de recursos minerales de Andalucía*, IGME-Junta Andalucía, Madrid, 108-190.

Main-Knorn, M., Pflug, B., Louis, J., Debaecker, V., Müller-Wilm, U., Gascon, F., 2017. *Sen2Cor For Sentinel-2*. 3. 10.1117/12.2278218.

Matos, J. X., Martins, L., 2006. Reabilitação ambiental de áreas mineiras do sector português da Faixa Piritosa Ibérica: estado da arte e perspectivas futuras. *Bol. Geológico y Minero España*, IGME, **117**(2): 289-304. ISSN 0366-0176.

Matos, J. X., Martins, L. P., Oliveira, J. T., Pereira, Z., Batista, M. J., Quental, L., 2008. Rota da pirite no sector português da Faixa Piritosa Ibérica, desafios para um desenvolvimento sustentado do turismo geológico e mineiro. Proj.RUMYS/CYTED, *Livro Rutas Minerales en Iberoamérica*, Ed. Paul Carrion, Esc. Sup. Politécnica del Litoral, Guayaquil, Equador: 136-155.

Matos, J. X., Pereira, Z., Fernandes, P., Rosa, D., Oliveira, J. T., 2010. Contribution to the understanding of the structure of Aljustrel mine Iberian Pyrite Belt, based in new palynostratigraphical data obtained in the Volcano-Sedimentary Complex and Mértola Formation. *VIII Congresso Nacional de Geologia, e-Terra*, 21, 10, 1-4.

Matos, J. X., Filipe, A. (Coords.), 2013. *Carta De Ocorrências Mineiras Do Alentejo e Algarve à Escala 1:400 000, Versão Digital*. Edição LNEG/ATLANTERRA, Lisboa. ISBN: 978-989-675-029-9.

Matos, J. X., Carvalho, J., Represas, P., Batista, M. J., Sousa, P., Ramalho, E. C., Marques, F., Morais, I., Albardeiro, L., Gonçalves, P., Dias, P., 2020. Geophysical surveys in the Portuguese sector of the Iberian Pyrite Belt: a global overview focused on the massive sulphide exploration and geologic interpretation. *Comunicações Geológicas*, **107**(III): 41-78.

Mylona, E., Daskalopoulou, V., Sykioti, O., Koutroumbas, K., Rontogiannis, A., 2018. Classification of Sentinel-2 Images Utilizing Abundance Representation. *Proceedings*, **2**: 328.

NASA, 2016. *Landsat 7 Science Data Users Handbook*. Https://Landsat.Gsfc.Nasa.Gov/Wp-Content/Uploads/2016/08/Landsat7_Handbook.Pdf.

Oliveira, J. T., Relvas, J., Pereira, Z., Matos, J. X., Rosa, C., Rosa, D., Munhá, J. M., Fernandes, P., Jorge, R., Pinto, A., 2013. Geologia da Zona Sul Portuguesa, com ênfase na estratigrafia e na vulcanologia física, geoquímica e mineralizações da Faixa Piritosa. *In*: Dias, R., Araújo, A., Terrinha, P., Kullberg, J. (Eds.), *Geologia de Portugal Vol. I - Geologia Pré-mesozóica de Portugal*, Escolar Editora, 673 - 767.

Park, S.; Choi, Y. Applications of Unmanned Aerial Vehicles in Mining from Exploration to Reclamation: A Review. *Minerals*, 10, 663.

Pinedo-Vara, 1963. *Piritas de Huelva, su historia, minéria y aprovechamiento*. Ed. Summa, Madrid, 1003.

Quental, L., Sousa, A. J., Marsh, S., Abreu, M. M., 2013. Identification of Materials Related to Acid Mine Drainage Using Multi-Source Spectra at S. Domingos Mine, Southeast Portugal. *International Journal of Remote Sensing*, **34**(6): 1928-1948

Quental, L. Sousa, A. J, Marsh, S., Brito, G. Abreu, M. M., 2011a. Imaging Spectroscopy Answers to Acid Mine Drainage Detection at S. Domingos, Iberian Pyrite Belt, Portugal. *Comunicações Geológicas*, **98**: 61-71. Http://Hdl.Handle.Net/10400.9/1444

Quental L., Sousa A. J, Marsh, S., 2011b. Low PH Detection in Specim Eagle-Hawk Using Field Spectra at S. Domingos Mine, SE Portugal: Preliminary Results. *3rd Workshop on Hyperspectral Image and Signal Processing: E(2011c) Evolution in Remote Sensing (WHISPERS), 6-9 June*, Lisbon, Portugal. 4.

Quental, L., 2011. *Comparison of Calibration of Hyperspectral Image-Processing Techniques For Environmental Assessment In S. Domingos Mine, SE Portugal*. PhD Thesis, Instituto Superior Técnico, 176.

Quental, L., Batista, M. J, Oliveira, D., Matos J. X., Dias, R., Gonçalves, P., 2018. Sentinel 2 And Radiometric Data as Geological and Mineral Exploration Characterization Tools. Southern Portugal / Sentinel 2 E

Dados Radiométricos Para Caracterização Geológica E De Prospeção No Sul De Portugal. (XCNG-17743). *Vulcânica*, **II**: 167-168. ISSN 1646-3269.

Quental, L., Sousa, A. J., Marsh, S. Brito, G., Abreu, M. M., 2012. Remote Sensing for Waste Characterisation. *In*: Batista, M. J. *et al.* (Eds.), *FIELD TRIP GUIDEBOOK: Multidisciplinary contribution for environmental characterization and improvement at the S. Domingos mining site*. Chapter: Remote sensing for waste characterization, 9th Int. Symp. Environ. Geochem, Aveiro, Portugal, 18-24.

Quental, L. Bourguignon, A., Sousa, A. J., Batista, M. J., Brito, M. G. Tavares, T. Abreu, M. M., Vairinho, M. M., Cottard, F., 2002. MINEO Southern Europe Environment Test Site: Contamination *Impact Mapping and Modelling. Final Report of the MINEO Project - Assessing and Monitoring the Environmental Impact of Mining In Europe Using Advanced Earth Observation Techniques*. 131. Http://Repositorio.Lneg.Pt/Handle/10400.9/3268

Quental, L. Matos, J., 2006. Land Cover Mapping Using Quickbird™ Imagery: Preliminary Results of the Mining Area of Aljustrel, Iberian Pyrite Belt. Proceedings *Of 5th European Congress on Regional Geoscientific Cartography and Information Systems Earth and Water*, Catalonia, Spain, **II**, 73-75.

Quental, L., 2006. *Deliverables of the e-EcoRisk project*: D32211-Image acquistion and processing 12p.D 32221-DEM, 8p. D32231-Image Analysis and Interpretation, 22. D32212- A set of fully processed and georeferenced images. D32232- Set of image interpretation maps, including NDVI; Land Cover.

Relvas, J. M. R. S., Pinto, A. M. M., Matos, J. X., 2012. Lousal, Portugal: a successful example of rehabilitation of a closed mine in the Iberian Pyrite Belt. *Society for Geology Applied to Mineral Deposits SGA News*, **31**: 1-16.

Roberts, D., Mueller, N., Mcintyre, A., 2017. High-Dimensional Pixel Composites from Earth Observation Time Series. *IEEE Transactions on Geoscience and Remote Sensing*, **55**(11): 6254-6264. http://Doi:10.1109/TGRS.2017.2723896

Schaepman, M. E., Green, R. O., Ungar, S., Boardman, J., Plaza, A. J., Gao, B. C., Ustin, S., Miller, J., Jacquemoud, S., Ben-Dor, E., Clark, R., Davis, C., Dozier, J., Goodenough, D., Roberts, D., Goetz, A. F. H., 2006. The Future of Imaging Spectroscopy – Prospective Technologies and Applications. *Proceedings of IEEE International Geoscience and Remote Sensing Symposium*. Denver: IEEE, 2005-2008.

Segal, D., 1982. Theoretical Basis for Differentiation of Ferric-Iron Bearing Minerals, Using Landsat MSS Data. *Proceedings of Symposium for Remote Sensing of Environment, 2nd Thematic Conference on Remote Sensing for Exploratory Geology, Fort Worth*, TX., 949-951.

Schaepman, M., Ustin, M., Plaza, A., Painter, T., Verrelst, J., Liang, S., 2009. Earth System Science Related Imaging Spectroscopy – An Assessment. *Remote Sensing of Environment*, **113**, S123–S137.

Szantoi, Z., Strobl, P., 2019. Copernicus Sentinel-2 Calibration and Validation. *European Journal of Remote Sensing*, **52**: 253. 10.1080/22797254.2019.1582840.

Tavares, M. T., Sousa, A. J., Abreu, M. M., 2008. Ordinary kriging and indicator kriging in the cartography of trace elements contamination in São Domingos mining site (Alentejo, Portugal). *Journal of Geochemical Exploration*, **98**: 43-56.

Tavares, M. T, Abreu, M. M, Vairinho, M. M., Sousa, A. J., Quental, L., 2009. Comportamento geoquímico de alguns elementos vestigiais na envolvente das Minas de S. Domingos, Alentejo: áreas da Tapada e do Telheiro. *Revista de Ciências Agrárias*, **32**(1): 182-194.

Tornos, F., 2006. Environment of formation and styles of volcanogenic massive sulfides: the Iberian Pyrite Belt. *Ore Geology Reviews*, **28**, 259-307. http://Doi:10.1016/j.oregeorev. 2004.12.005.

Vairinho, M., Couto, A., Batista, M. J., Ferreira, A., Quental, L., Matos, J. X., 2004. Interpretation of Landsat 7 ETM+ Imagery and Integration with Geochemical Data in Aljustrel – S. Domingos Area, Iberian Pyrite Belt, Portugal: A Regional Approach. *32nd International Geological Congress* – Florence, Italy.

Van Der Meer, F. D, Van Der Werff, H. M. A., Van Ruitenbeek, F. J. A., 2014. Potential of ESA's Sentinel-2 for Geological Applications. *Remote Sensing of Environment*, **148**: 124-133. ISSN 0034-4257, Https://Doi.Org/10.1016/J.Rse.2014.03.022.

Van Der Werff, H., Van Der Meer, F., 2016. Sentinel-2A MSI And Landsat 8 OLI Provide Data Continuity for Geological Remote Sensing. *Remote Sens.*, **8**: 883.

Vieira, A., Matos, J. X., Lopes, L., Martins, R., 2016. Tridimensional modelling and resource estimation of the mining waste piles of São Domingos mine, Iberian Pyrite Belt, Portugal. *Geophysical Research Abstracts*, **18**, EGU 2016, Abs.

Vieira, A., Matos, J.X., Lopes, L., Martins, R., 2020. Evaluation of the mining potential of the São Domingos mine wastes, Iberian Pyrite Belt, Portugal. *Comunicações Geológicas*, Explora, **107**(III): 91-100.